Date of publication xxxx 00, 0000, date of current version xxxx 00, 0000.

Digital Object Identifier 10.1109/ACCESS.201X.DOI

General Framework for the Efficient Optimization of Reflectarray Antennas for Contoured Beam Space Applications

DANIEL R. PRADO[1], JESÚS A. LÓPEZ FERNÁNDEZ[2], MANUEL ARREBOLA[2], (Senior Member, IEEE,) MARCOS R. PINO[2], AND GEORGE GOUSSETIS[1], (Senior Member, IEEE)

[1]Institute of Sensors, Signals and Systems, School of Engineering and Physical Sciences, Heriot-Watt University, Edinburgh, U.K. (e-mail: {dr38,G.Goussetis}@hw.ac.uk)

[2]Department of Electrical Engineering, Universidad de Oviedo, Gijón, Spain (e-mail: {jelofer,arrebola,mpino}@uniovi.es)

Corresponding author: Daniel R. Prado (e-mail: dr38@hw.ac.uk).

This work was supported in part by the European Space Agency (ESA) under contract ESTEC/AO/1-7064/12/NL/MH; by the Ministerio de Ciencia, Innovación y Universidades under project TEC2017-86619-R (ARTEINE); by the Ministerio de Economía, Industria y Competitividad under project TEC2016-75103-C2-1-R (MYRADA); by the Gobierno del Principado de Asturias through Programa "Clarín" de Ayudas Postdoctorales / Marie Courie-Cofund under project ACA17-09.

ABSTRACT This paper describes a general framework for the optimization of very large reflectarrays for space applications. It employs the generalized Intersection Approach (IA) as optimizing algorithm, integrating a number of techniques that substantially improve the baseline algorithm by accelerating computations while preserving the accuracy of the electromagnetic analysis. In particular, a learning algorithm based on Support Vector Machines (SVMs) is used to obtain a surrogate model of the reflectarray unit cell accelerating the analysis more than three orders of magnitude. For the optimization, the gradient computation is accelerated by employing the technique of differential contributions on the radiated field, which avoids the use of the Fast Fourier Transform (FFT) in the computation of the far field. Finally, to improve the cross-polarization performance, instead of optimizing the crosspolar pattern, the crosspolar discrimination or crosspolar isolation are optimized, improving both the antenna and algorithm performance. Relevant numerical examples are provided to show the capabilities of the proposed framework for a Direct Broadcast Satellite (DBS) mission, showing how to design a contoured beam reflectarray with a European footprint with two different coverage zones. In addition, a complete study of computing time is carried out to analyse the impact of each technique in the optimization process.

INDEX TERMS Very large reflectarray, radiation pattern synthesis, contoured beam, crosspolar optimization, machine learning technique, support vector machines, gradient-based algorithm, crosspolar discrimination (XPD), crosspolar isolation (XPI), Direct Broadcast Satellite (DBS)

I. INTRODUCTION

The constant development of communication technologies has resulted in the need of systems which fulfil increasing tighter requirements in order to improve their quality and performance. In particular, communications through satellites are commonplace in modern society, including applications such as television broadcast, mobile telephone networks and data transmission. In addition to communication satellites, other space applications include radar, navigation and remote sensing [1]. In all of them, the antenna is a very important subsystem, since it allows wireless communications, converting guided waves into radiating waves propagating in free space, and vice versa. Depending on the application, different parameters may be optimized, including but not limited to efficiency, size, matching and radiation pattern. Specifically, radiation pattern synthesis is important for both terrestrial and space application, since non-canonical beam patterns are not easy to achieve [2]. Furthermore, within antenna pattern synthesis, copolar shaped patterns are easier to obtain compared with crosspolar far field optimization. Some applications that demand shaped beams include global Earth coverage, which requires an isoflux pattern providing constant

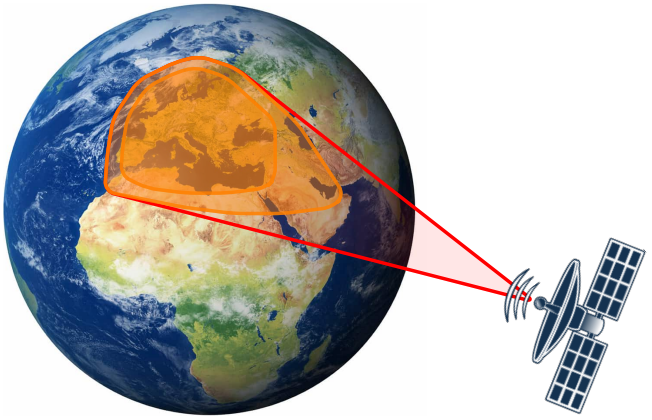

FIGURE 1. Illustration of a satellite in geostationary orbit providing DBS service with a European footprint having several coverages zones with different requirements.

energy flux on the surface of the Earth [3]; Direct Broadcast Satellite (DBS) applications, which require a shaped beam to fulfil a given footprint on the Earth Surface (see Fig. 1); etc. DBS applications are particularly challenging since they also require a high polarization purity, working with very large antennas. Traditionally, shaped parabolic reflectors have been used for this kind of applications [1]. However, they are bulky and expensive, and with the popularization of the microstrip technology reflectarrays have become a potential substitute to parabolic reflector dishes [2].

A reflectarray consists of a primary feed, typically a horn antenna, and an array of radiating elements, which add a certain phase-shift on the reflected wave (see Fig. 2). They are usually comprised of hundreds or even thousands of elements, making antenna pattern synthesis a very challenging task when dealing with very large reflectarrays. This is especially true for applications with very stringent requirements, such as Direct Broadcast Satellite (DBS) missions [1], [2]. In addition, current applications such as multibeam [4] or Synthesis Radar Aperture (SAR) [5] are proposing ever-larger reflectarrays, with very high gain and narrow beams which are driving current analysis and optimization techniques to face memory and computational limitations due to the large number of elements involved and the high resolution necessary to correctly characterize the radiation pattern.

The optimization of reflectarray antennas has been a challenge in recent years. The dominant synthesis approach consists in a Phase-Only Synthesis (POS) that employs a simplified analysis of the reflectarray unit cell to accelerate computations. In POS, the unit cell is considered an ideal phase-shifter with no losses and no cross-polarization [6]. These simplifications barely affect the copolar pattern [7], but the crosspolar pattern computed is not valid. Thus, POS techniques are only able to deal with copolar requirements [6]–[8]. The goal of the POS is to obtain a phase distribution that generates the desired copolar pattern according to certain requirements. Then, the reflectarray layout is obtained using a Full-Wave analysis tool based on Local Periodicity (FW-LP), usually a Method of Moments (MoM-LP) and a zero-finding routine which adjusts the geometry of each unit cell to match the required phase-shift [2]. The simulated layout using a FW-LP will produce the desired copolar pattern as obtained from the POS plus a small gain loss which depends on the selected substrate. However, since the crosspolar pattern was not taken into account during the synthesis, it may not comply with the expected cross-polarization performance, which will depend on the application.

The crosspolar optimization was first handled at a unit cell level [9]–[13] since the direct optimization of the whole reflectarray was considered impractical [14]. An early work [9] proposed an arrangement of the reflectarray elements in four quadrants with mirror symmetry to reduce the crosspolar pattern. This approach was later improved in [10], where the mirror-like arrangement was imposed among neighbour elements, and showed better performance than that of [9]. Another technique was presented in [11] and later implemented in [12]. It consists in enforcing a null in the amplitude of the reflection cross-coefficients that contribute more to the crosspolar pattern. Element rotation was employed in [13] to minimize the crosspolar tangential field at the reflectarray aperture, thus reducing the crosspolar pattern indirectly. For this reason, working at the element level provides suboptimal results.

A more flexible approach to the crosspolar optimization is to work at the radiation pattern level, optimizing all the reflectarray elements at the same time. In this regard, some techniques have been developed that allow the direct optimization of reflectarray antennas considering both copolar and crosspolar requirements. One of the first works to perform direct optimization was presented in [15]–[17]. However, it only considered single-polarized reflectarrays with very few elements (a total of 225) and the algorithm was slow. In [18], an efficient extension of the Intersection Approach algorithm was presented, giving as a result a distribution of reflection coefficient matrices (instead of a phase distribution). The main drawback was to obtain a reflectarray layout from such matrices, which is a challenging task. Nevertheless, a similar approach was followed in [19], and the layout was obtained by applying trapezoidal transformations to the unit cell. In [20] a gradient minimax algorithm was used, accelerating computations with the use of a database of the scattering matrix of the reflectarray unit cell. In [21] the direct optimization employs a full-wave analysis based on local periodicity, in particular a MoM-LP, making computations slow. However, the algorithm is able to handle thousands of optimizing variables with success and a number of techniques were introduced to minimize the number of calls to the MoM-LP routine and to accelerate computations.

In this paper, we present a general framework for the efficient optimization of very large reflectarrays including copolar and crosspolar requirements, focusing on space applications where the specifications are very tight. The chosen algorithm is the generalized Intersection Approach, which

integrates a number of techniques that substantially improve the baseline algorithm from the point of view of the antenna and algorithm performances. First, the reflectarray analysis is presented, with an efficient formulation taking into account a spatial shift which may cause a pointing error in the far field if it is not considered. Then, the MoM-LP is replaced with a machine learning algorithm, SVM, to greatly accelerate the analysis time while keeping a high degree of accuracy with regard to the electromagnetic tool simulations. Thanks to the use of the SVM, the analysis and layout design of a very large reflectarray comprised of several thousand elements are accelerated more than three orders of magnitude. Next, the computation of the gradient is considerably accelerated by employing differential contributions to the far field, thanks to the linearity of Maxwell's equations, which provides a linear relationship between the tangential field at the aperture and the radiated field (either near or far field). This approach is most useful when the radiation pattern employs fine grids, which is necessary in very large arrays with high directivity. In addition, most space applications impose very tight cross-polarization requirements. By directly optimizing the cross-polarization figure of merit instead of the crosspolar far field (for instance, the crosspolar discrimination in DBS applications), the optimization is accelerated and the antenna performance is improved. Finally, the presented framework is used to design a reflectarray for a DBS application with European coverage, starting from an efficient phase-only synthesis and layout design using SVM, to a cross-polarization performance optimization using the generalized Intersection Approach, employing all the techniques previously introduced. A thorough computational time study is carried out to assess the impact of the techniques in the crosspolar optimization algorithm.

The paper is organized as follows. Section II presents the efficient analysis of reflectarray antennas, including the formulation for the displacement of phase-shifters and cell modelling with SVM. Section III presents the optimization algorithm and the technique of differential contributions to accelerate the gradient computation. Section IV shows an efficient procedure to design a contoured beam reflectarray for DBS applications. In Section V, the results of the crosspolar optimization using all previous techniques are presented, as well as a thorough computing time study to asses the impact of those techniques in the optimization algorithm. Finally, Section VI contains the conclusions.

II. EFFICIENT ANALYSIS OF REFLECTARRAYS

A. CLASSIC APPROACH

Fig. 2 shows a sketch of the single-offset reflectarray geometry under consideration. It consists of a planar reflectarray illuminated by a feed, usually a horn antenna, which generates a tangential incident field on the reflectarray surface:

$$\vec{E}_{\text{inc}}^{X/Y}(x,y) = E_{\text{inc},x}^{X/Y}(x,y)\,\hat{x} + E_{\text{inc},y}^{X/Y}(x,y)\,\hat{y}, \tag{1}$$

where the superscript indicates the linear polarization of the horn antenna, the subscript the component of the field

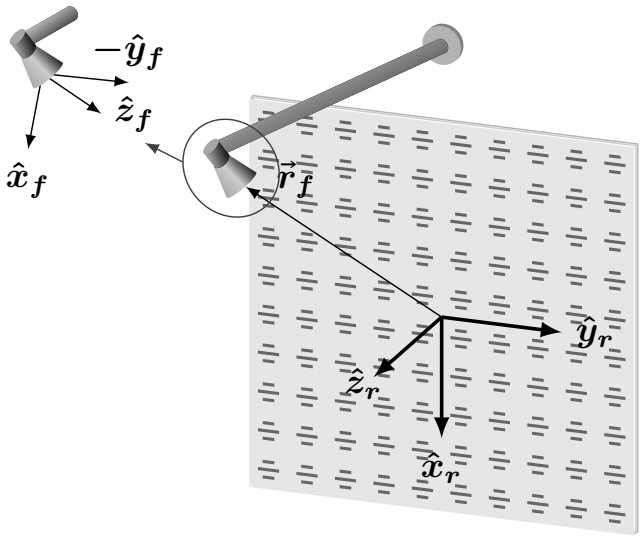

FIGURE 2. Sketch of the single-offset reflectarray geometry under study.

with regard to the reflectarray coordinate system (see Fig. 2) and (x,y) is a point in the reflectarray surface. Only the tangential field at the aperture is of interest to later compute the radiation pattern. On the other hand, the reflected field is obtained, at each reflectarray element, as:

$$\vec{E}_{\text{ref}}^{X/Y}(x_k,y_k) = \mathbf{R}_k \cdot \vec{E}_{\text{inc}}^{X/Y}(x_k,y_k), \tag{2}$$

where (x_k,y_k) are the coordinates of the kth element and $\mathbf{R}_k$ is a 2×2 matrix known as the reflection coefficient matrix:

$$\mathbf{R}_k = \begin{pmatrix} \rho_{xx,k} & \rho_{xy,k} \\ \rho_{yx,k} & \rho_{yy,k} \end{pmatrix}. \tag{3}$$

The reflection coefficients do not depend on the polarization of the feed. For a given feed polarization and oblique incidence, the incident field presents two tangential components $\hat{x}$ and $\hat{y}$ as expressed by (1), which then will be multiplied by (3) to obtain the tangential reflected field. The reflection coefficients are complex numbers that characterize the behaviour of the unit cell in a periodic environment. ρ_{xx} and ρ_{yy} are known as the direct coefficients, and they control the shape of the copolar pattern through their phases and the losses through their magnitude. On the other hand, ρ_{xy} and ρ_{yx} are the cross-coefficients and considerably contribute to the crosspolar pattern. Matrix $\mathbf{R}_k$ is computed with a FW-LP tool [2] and the value of the reflection coefficients depends on several parameters, such as the unit cell geometry, frequency, periodicity, angle of incidence of the impinging wave and substrate properties. The magnetic tangential field is easily obtained from (2) following [21].

Once the tangential reflected field has been obtained with (2), the far field in spherical coordinates may be computed according to the first principle of equivalence in electromagnetics, also known as Love's equivalence principle [22]. For

this purpose, the spectrum functions are computed as the Fourier transform of the tangential field at the aperture:

$$P_{x/y}^{X/Y}(u,v) = \iint_S E_{\text{ref},x/y}^{X/Y}(x,y)\, e^{jk_0(ux+vy)}\, dx\,dy,$$
$$Q_{x/y}^{X/Y}(u,v) = \iint_S H_{\text{ref},x/y}^{X/Y}(x,y)\, e^{jk_0(ux+vy)}\, dx\,dy, \tag{4}$$

where $u = \sin\theta\cos\varphi$, $v = \sin\theta\sin\varphi$; S is the surface of the aperture and k_0 is the wavenumber in vacuum. The reflected magnetic field can be obtained from (2) assuming a locally incident plane wave coming from the feed as in [21]. In addition, the integrals in (4) may be efficiently evaluated with the FFT algorithm [2]. Finally, the copolar and crosspolar components are obtained using Ludwig's third definition of cross-polarization. Explicit transformation matrices from spherical to copolar and crosspolar components for both linear polarizations may be found in [18].

B. ANALYSIS CONSIDERING UNIT CELLS WITH PHYSICAL DISPLACEMENT OF PHASE-SHIFTERS

The unit cell is an important factor for the reflectarray performance. In particular, the unit cell should provide enough phase-shift to perform a layout design, low losses and low cross-polarization. In addition, decoupling between polarizations would facilitate the design, since each polarization could be controlled independently. An adequate unit cell is the one proposed in [23] and shown in Fig. 3. This cell is comprised of two sets of four parallel dipoles in two different layers, one for each linear polarization. The set of four dipoles oriented in $\hat{x}$ controls the phase shift for polarization X, while the set oriented in $\hat{y}$ controls the phase shift for polarization Y. In addition, both sets of dipoles are shifted half a period in order to give enough room for the dipoles to provide a large phase shift by increasing their length while avoiding overlapping. The FW-LP tool which analyses the cell is the Method of Moments based on Local Periodicity (MoM-LP) described in [24], which has been extensively validated by full-wave simulations of the whole antenna [13] as well as with prototype measurements [23], [25]–[27]. This unit cell has been chosen since it provides low cross-polarization and a large phase-shift range with enough degrees of freedom to perform reflectarray optimization [21], [23].

As it can be seen in Fig. 3, the phasing cell of the reflectarray element in one polarization is shifted by half a period with respect to the orthogonal polarization. This shift has to be taken into account in the illumination of the reflectarray by considering that the positions of the dipoles oriented in the $\hat{y}$ axis are displaced half a period with respect to the other set of dipoles. If this spacial shift is not taken into account, the pointing direction of the main beam is not well predicted when comparing simulations with measurements [27]. Although the shift in the main beam is small, it may have a significant impact for highly directive antennas, as it will be shown later. Taking as reference the phase shifter for polarization X (in the case of the chosen unit cell, the dipoles oriented in $\hat{x}$), let (x,y) be its reference coordinates. Then, the reference coordinates of the phase shifter for polarization Y (x',y') are related to (x,y) through:

$$x' = x + \Delta x,$$
$$y' = y + \Delta y. \tag{5}$$

With this correction, (2) is modified as follows [27]:

$$\begin{pmatrix} E_{\text{ref},x}^{X/Y} \\ E_{\text{ref},y}^{X/Y} \end{pmatrix} = \mathbf{R}_k \begin{pmatrix} E_{\text{inc},x}^{X/Y}(x_k,y_k)\,\big|_{\text{on pol. X dipoles}} \\ E_{\text{inc},y}^{X/Y}(x'_k,y'_k)\,\big|_{\text{on pol. Y dipoles}} \end{pmatrix}. \tag{6}$$

Since the incident field is obtained at different spatial coordinates for each component, they cannot be directly added to form the reflected field. In this regard, (6) incurs on abuse of notation and this will be fixed shortly. Instead, the contributions from each phase-shifter will be added in the far field. Please note that the reflection coefficients in (3) are the same for both reference coordinates since they are computed assuming local periodicity.

In this way, using (6) in (4) for the electric field it follows:

$$P_x^{X/Y} = \iint_{S_1} \rho_{xx} E_{\text{inc},x}^{X/Y}(x,y) e^{jk_0(ux+vy)}\, dx\,dy + \iint_{S_2} \rho_{xy} E_{\text{inc},y}^{X/Y}(x',y') e^{jk_0\left(ux'+vy'\right)}\, dx'\,dy', \tag{7}$$

$$P_y^{X/Y} = \iint_{S_1} \rho_{yx} E_{\text{inc},x}^{X/Y}(x,y) e^{jk_0(ux+vy)}\, dx\,dy + \iint_{S_2} \rho_{yy} E_{\text{inc},y}^{X/Y}(x',y') e^{jk_0\left(ux'+vy'\right)}\, dx'\,dy'. \tag{8}$$

Each integral is calculated in different integration surfaces, S_1 and S_2 as illustrated in Fig. 4. To compute (7) and (8) with the FFT as in [2] both integrals need to be related to the same coordinates. Thus, considering (5) and after a few operations it follows:

$$P_x^{X/Y} = \iint_{S_1} \rho_{xx} E_{\text{inc},x}^{X/Y}(x,y) e^{jk_0(ux+vy)}\, dx\,dy + e^{jk_0(u\Delta x+v\Delta y)} \iint_{S_1} \rho_{xy} E_{\text{inc},y}^{X/Y}(x',y') e^{jk_0(ux+vy)}\, dx\,dy, \tag{9}$$

$$P_y^{X/Y} = \iint_{S_1} \rho_{yx} E_{\text{inc},x}^{X/Y}(x,y) e^{jk_0(ux+vy)}\, dx\,dy + e^{jk_0(u\Delta x+v\Delta y)} \iint_{S_1} \rho_{yy} E_{\text{inc},y}^{X/Y}(x',y') e^{jk_0(ux+vy)}\, dx\,dy. \tag{10}$$

Now, each spectrum function may be computed with two FFTs instead of one due to the spatial shift between the two sets of dipoles. As a consequence, the spectrum functions computation time is doubled, although a more accurate analysis of the reflectarray radiation pattern is achieved [27]. It must be highlighted that now the integrals in (9) and (10) are only integrated in surface S_1 so the FFT may be employed, but the $\hat{y}$ component of the incident field is obtained in the (x',y') coordinates, which depend on (x,y) through (5).

The procedure for the magnetic field spectrum functions is analogous. Once they have been obtained, the copolar and crosspolar components may be readily calculated following [18].

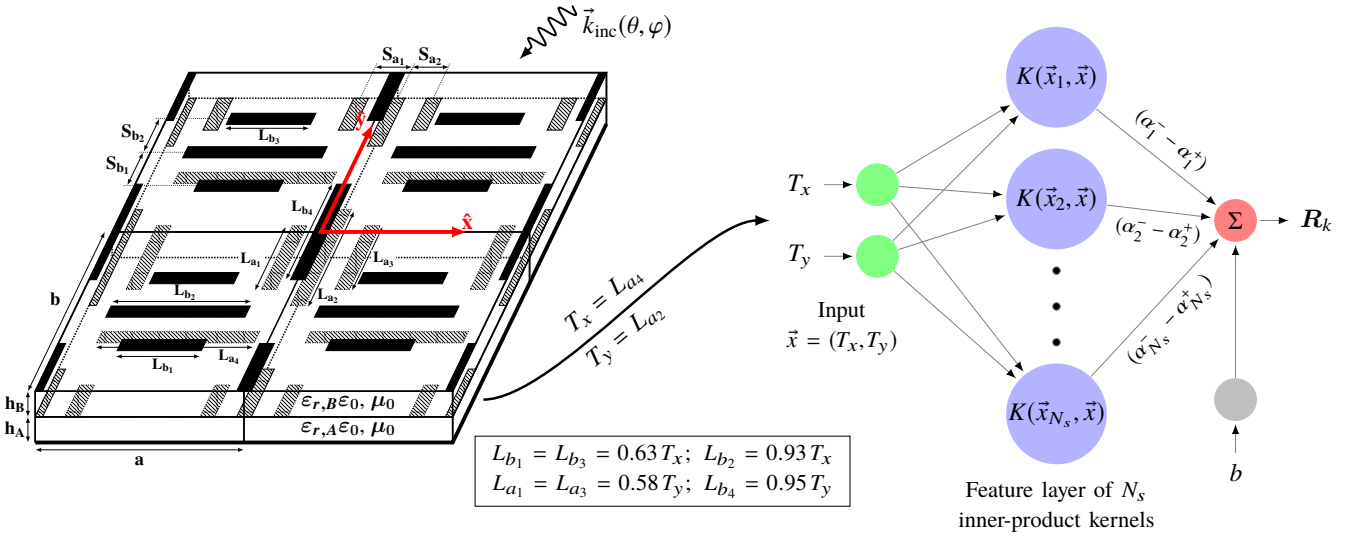

FIGURE 3. Sketch of the reflectarray unit cell and the construction of the reflection coefficients matrix $\mathbf{R}_k$ using the SVM. The unit cell is comprised of two sets of parallel dipoles, one controlling polarization X (dipoles oriented in $\hat{\mathbf{x}}$) and another controlling polarization Y (dipoles oriented in $\hat{\mathbf{y}}$), in two different layers (black dipoles in the top layer and gray dipoles in the middle layer) backed by a ground plane (bottom layer). For the SVM training, only two geometrical variables are considered, T_x and T_y, with the lengths of the dipoles proportional to them as in [26]. Then, T_x and T_y are the input variables of the SVM, whose output is the electromagnetic response of the unit cell for a given angle of incidence (θ,φ) of the impinging plane wave, i.e., the reflection coefficient matrix $\mathbf{R}_k$, whose elements are obtained as a linear combination of the SVM kernels.

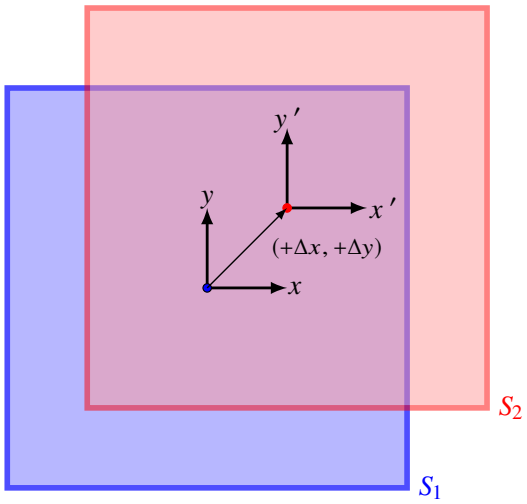

FIGURE 4. Illustration of the physical displacement effect of the phase-shifters on the integration surface to compute the spectrum functions.

C. SURROGATE MODEL OF THE UNIT CELL

Following the steps detailed above, the calculation of the $\mathbf{R}_k$ matrix in (3) with a FW-LP tool is the most time consuming step in the radiation pattern computation. Thus, for an efficient optimization process, where the reflectarray analysis is performed hundreds or even thousands of times, it is interesting to accelerate the computation of $\mathbf{R}_k$. In this work, the chosen strategy is to model the behaviour of the unit cell with a machine learning algorithm known as Support Vector Machine (SVM) [28].

SVMs are automatic and supervised learning algorithms which are used to solve regression and classification problems. In the present case, the SVM regression characteristics are adapted to seek a surrogate model of the unit cell. A complete description of the SVM theory background and training strategies may be found in [29]. Only the basic features will be described here for completeness.

Given a training set of inputs and outputs, $S = \{\vec{x}_i, y_i\}_{i=1,2,\ldots,N_r}$, with $\vec{x}_i \in \chi \subseteq \mathbb{R}^L$ and $y_i \in \mathbb{R}$, the SVM is used to obtain a function f which estimates the output $\tilde{y}$ that corresponds to a new input $\vec{x}$ as:

$$\tilde{y} = f(\vec{x}), \tag{11}$$

where f follows the expression:

$$f(\vec{x}) = b + \sum_{i=1}^{N_s} \left[\left(\alpha_i^- - \alpha_i^+\right) K(\vec{x}_i, \vec{x}) \right], \tag{12}$$

and b is known as the offset, N_s is the total number of support vectors, α_i^+ and α_i^- are the optimal Lagrange multipliers, and K is the kernel function, which in the present case is a Gaussian kernel:

$$K(\vec{x}, \vec{x}') = \exp\left(-\gamma \|\vec{x} - \vec{x}'\|^2\right), \tag{13}$$

where $\|\cdot\|$ is the Euclidean norm and γ a tunable parameter. Therefore, function f may be interpreted as a linear combination of Gaussian functions placed at the support vectors plus an offset, where the width of the Gaussian functions is inversely proportional to γ.

The obtained function f in (12) minimizes a regularized risk functional that accounts for the empirical errors (weighted by a tunable parameter C) and for the flatness of f in the feature space (or its smoothness in the input space). On the one hand, when the flatness is maximized, f has good

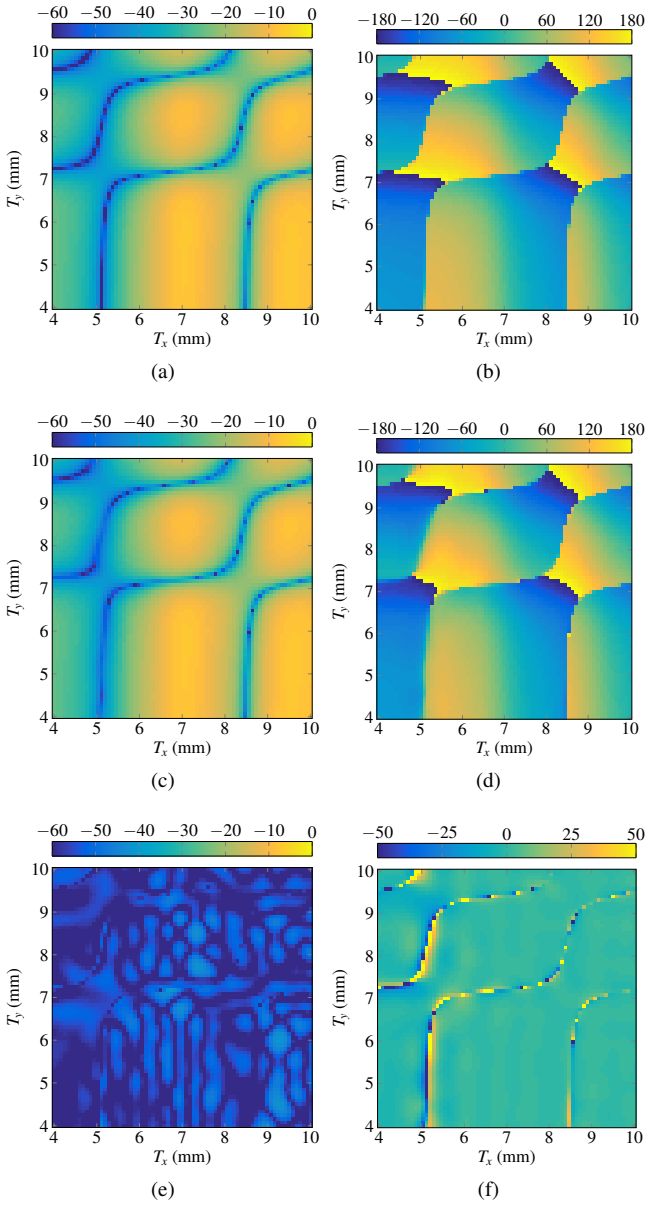

FIGURE 5. For the reflection coefficient ρ_{yx} with $(\theta = 35°, \varphi = 35°)$, comparison between (a), (b) the MoM-LP simulation and (c), (d) SVM simulation for the (a), (c) magnitude in dB and (b), (d) phase in degrees. Difference of the (e) magnitude is in dB and of the (f) phase in degrees.

generalization properties. On the other hand, the empirical errors (absolute difference between the value of the output training samples and the output of the regression function) are the metric for how well it fits the training samples. Thus C provides a trade-off between the two. The parameters γ and C determine the shape of function f and must be carefully selected through a grid search in the (C, γ) plane [29].

The SVM is used to obtain the surrogate model of the reflection coefficients matrix $\mathbf{R}_k$ for the chosen unit cell (see Fig. 3). As in [29], only two geometric variables are considered, T_x and T_y, and the length of the dipoles will be proportional to those variables, as specified in Fig. 3. In addition, one SVM will be trained per angle of incidence (θ, φ). Due to the low losses the direct coefficients ρ_{xx} and ρ_{yy} are smooth as a function of T_x and T_y, and thus the regression error is very low. It is more difficult to obtain an accurate surrogate model of the cross-coefficients. Fig. 5 shows a comparison in magnitude and phase of the cross-coefficient ρ_{yx} for an oblique angle of incidence $(\theta = 35°, \varphi = 35°)$. The magnitude difference is very low, always below -40 dB. However, the phase difference shows high values where there are abrupt changes which the SVM simulation tends to soften. In any case, the mean absolute deviation (MAD) is 4° for this case, and 4.5° for the phase of ρ_{xy}, which are considered very low values for a cross-coefficient (for the phases of ρ_{xx} and ρ_{yy} the MAD is lower than 0.6°). The average relative error of the training for all reflection coefficients is -33 dB following [29, eq. (11)], which will provide a high degree of accuracy in the predicted radiation patterns. This average relative error has been computed for the real and imaginary part of all trained reflection coefficients over all the considered incident angles.

Finally, it has been opted for a 2D problem to achieve a highly accurate SVM model. In light of the results of other works in the literature dealing with machine learning algorithms in higher dimensions, it may be possible the use of SVMs to increase the number of available degrees of freedom for reflectarray optimization. Nevertheless, as it will be shown in Section V, the improvement of the achieved results with two variables per element is significant with regard to the starting point.

III. OPTIMIZATION FRAMEWORK FOR VERY LARGE REFLECTARRAYS

A. GENERALIZED INTERSECTION APPROACH

In this section, the optimization algorithm for very large reflectarrays is presented. It is based on the framework provided by the generalized Intersection Approach (IA) presented in [30] and particularized for reflectarray antennas in [21]. Fig. 6 shows a schematic flowchart of the algorithm. Starting from the initial layout (or phase distribution for a phase-only synthesis), it applies iteratively two operations: the forward and the backward projections. In the forward projection, the far field is computed and trimmed according to some specification templates given in the form of upper and lower masks. Then, in the backward projection the trimmed pattern is employed as reference for a local optimization procedure. This process is repeated until the algorithm has converged.

The generalized IA can be employed either for phase-only synthesis (POS) or to perform direct optimization of the layout. For POS, the target is to obtain phase distributions for the direct coefficients ρ_{xx} and ρ_{yy}. In this case, the reflectarray unit cell is modelled as an ideal phase shifter with no losses and no crosspolarization, in such a way that the optimization of the copolar far field is independent for both linear polarizations, as detailed in [31]. These simplifications made in the reflectarray unit cell analysis produce a computationally very

efficient and fast algorithm, which along with the improved convergence properties of the generalized IA [32] allows to perform copolar synthesis in a fast and reliable fashion. As a drawback, the crosspolar pattern is not correctly characterized with this methodology, and thus there is no control over it during the synthesis process. Once the phase distributions that radiate the required copolar pattern are obtained, the dimensions of the dipoles are adjusted using T_x and T_y to match the phase shift of ρ_{xx} and ρ_{yy}, respectively, using a zero finding routine [2]. A complete mathematical description of the generalized IA for reflectarray POS may be found in [6], using the Levenberg-Marquardt Algorithm (LMA) [31] as the local optimizer in the backward projection.

On the other hand, the work presented in [21] for crosspolar optimization employed a MoM-LP as analysis technique to obtain an accurate prediction of the electromagnetic behaviour of the unit cell. However, that version of the algorithm increases its computational cost due to the MoM-LP, and thus makes it unfeasible to optimize very large reflectarrays unless workstations are employed. In any case, the good convergence properties of the algorithm allows to handle tens of thousands of optimizing variables while obtaining good results. This is done by minimizing the number of local minima by working with the squared field amplitude (or equivalently the gain) and performing the optimization in several steps, increasing the number of optimizing variables as suggested in [30].

From a computational point of view, despite the computational improvements introduced to the generalized IA in [21], [31], there is still room for further improvements. For instance, the use of SVMs instead of MoM-LP will substantially accelerate the computation of the cost function and Jacobian matrix. However, the acceleration of the latter is limited since each column of the Jacobian only analyses one reflectarray element, while for the radiation pattern computation several FFTs are needed. For that reason, it is proposed to accelerate the computation of the Jacobian matrix by employing the technique of differential contributions to calculate the radiated field in each derivative. This technique is the subject of the next subsection.

B. ACCELERATING JACOBIAN MATRIX COMPUTATION WITH DIFFERENTIAL CONTRIBUTIONS

When doing POS, there is a direct expression relating the optimizing variables and the cost function which is relatively easy to derive analytically [33], [34]. However, this is not the case when doing a direct optimization of the layout for crosspolarization improvement, and finite differences must be used [20], [21], which slows the computation of the gradient (Jacobian matrix). Thus, it is interesting to accelerate the computation of the gradient, which is typically the most time consuming operation in the optimization process.

There are a number of possibilities to accelerate the computation of the gradient. The Adjoint Variable Method (AVM) is a class of techniques that allow to compute the derivatives with regard to any number of optimizing variables with only two simulations of the whole structure [35]. However, it typically deals with S parameters [36], [37], and it may not still be used for pattern synthesis [36]. Another technique, specifically developed for array antenna pattern synthesis, is the technique of differential contributions (DFC) [38]. It accelerates the computation of the derivative by only considering the differential contribution of the modified element. This is possible thanks to the linearity of Maxwell's equations, which provides a linear relation between the tangential field at the aperture and the radiated field (either near or far field).

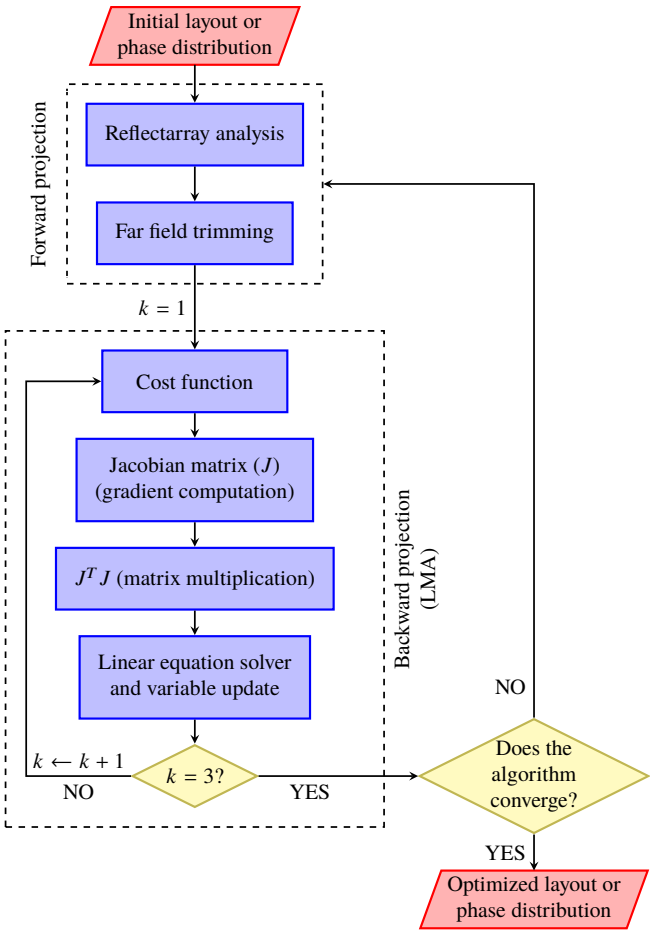

FIGURE 6. Flowchart of the generalized Intersection Approach particularized for the optimization of reflectarray antennas.

The Jacobian matrix may be formed with the gradient of a multidimensional scalar cost function of the form:

$$\nabla R(\vec{r},\bar{\xi}) = \left(\frac{\partial R(\vec{r},\bar{\xi})}{\partial \xi_1}, \cdots, \frac{\partial R(\vec{r},\bar{\xi})}{\partial \xi_i}, \cdots, \frac{\partial R(\vec{r},\bar{\xi})}{\partial \xi_P} \right), \tag{14}$$

where $\bar{\xi} = (\xi_1, \ldots, \xi_i, \ldots, \xi_P)$ is a vector of P optimizing variables and $\vec{r} \in \{\vec{r}_1, \ldots, \vec{r}_t, \ldots, \vec{r}_T\}$ an observation point where the radiated field is computed. For the case of the far field, $\vec{r}_t = (u, v)_t$ and since the generalized IA uses the LMA as the minimizing algorithm, R is the residual of the cost function [31]. When there is no analytical expression to calculate each

derivative, they are computed using finite differences. Using a backward lateral difference, the derivative is:

$$\frac{\partial R(\vec{r},\bar{\xi})}{\partial \xi_i} = \frac{R(\vec{r},\bar{\xi}) - R(\vec{r},\bar{\xi} - h\hat{e}_i)}{h} + \mathscr{O}(h), \qquad (15)$$

where h is a small positive scalar and $\hat{e}_i$ is the i th unit vector. To alleviate notation, henceforth we drop the dependence on $\vec{r}$ to focus on the optimization variables $\bar{\xi}$.

For the computation of the derivative by means of (15), the residual $R(\bar{\xi})$ depends on the far field $\vec{E}_{\text{ff}}(\bar{\xi})$ and it is common to all P derivatives in (14), so it is only computed once. On the other hand, $R(\bar{\xi} - h\hat{e}_i)$ depends on $\vec{E}_{\text{ff}}(\bar{\xi} - h\hat{e}_i)$, and is computed for each derivative. Since the reflectarray analysis assumes local periodicity, the modification of one element (variable) does not affect the others, and the perturbed field may be computed with the differential contribution:

$$\vec{E}_{\text{ff}}(\bar{\xi} - h\hat{e}_i) = \vec{E}_{\text{ff}}(\bar{\xi}) + \Delta\vec{E}_{\text{ff}}(\xi_i), \qquad (16)$$

where $\Delta\vec{E}_{\text{ff}}(\xi_i)$ is the differential contribution to the far field produced by the reflectarray element depending on variable i:

$$\Delta\vec{E}_{\text{ff}}(\xi_i) = \vec{E}_{\text{ff}}(\xi_i - h) - \vec{E}_{\text{ff}}(\xi_i). \qquad (17)$$

Thanks to the linearity of Maxwell's equations, there exists a linear dependence of the radiated field (either near or far field) at each point with respect to each contribution of the tangential field at the aperture. If we denote by $\vec{E}_{\text{ref},k}(\xi_i)$ the reflected tangential field of element k and depending on variable ξ_i, (17) can be expressed writing the radiated field as a function of the tangential field:

$$\Delta\vec{E}_{\text{ff}}(\xi_i) = \vec{E}_{\text{ff}}(\vec{E}_{\text{ref},k}(\xi_i - h)) - \vec{E}_{\text{ff}}(\vec{E}_{\text{ref},k}(\xi_i)). \qquad (18)$$

Since the radiated field is linear with respect to the tangential field:

$$\Delta\vec{E}_{\text{ff}}(\xi_i) = \vec{E}_{\text{ff}}(\Delta\vec{E}_{\text{ref},k}(\xi_i)), \qquad (19)$$

where:

$$\Delta\vec{E}_{\text{ref},k}(\xi_i) = \vec{E}_{\text{ref},k}(\xi_i - h) - \vec{E}_{\text{ref},k}(\xi_i). \qquad (20)$$

Thus, (19) indicates that to compute one derivative, only the differential contribution of one element is necessary. In practise, this means that, starting from the tangential field, the time cost of computing the far field is reduced from $\mathscr{O}(T \log T)$ when using the FFT to $\mathscr{O}(T)$ using the Differential Contributions (DFC) technique in the computation of each derivative [38]. The impact of this technique in the optimization process will be analysed in Section V.

IV. DESIGN OF A CONTOURED BEAM REFLECTARRAY

This section employs the generalized IA described in Section III to perform the design of a contoured beam reflectarray for DBS application with a European coverage. The SVM is employed to greatly accelerate the layout design, achieving speed up factors greater than three orders of magnitude for the analysis and layout design.

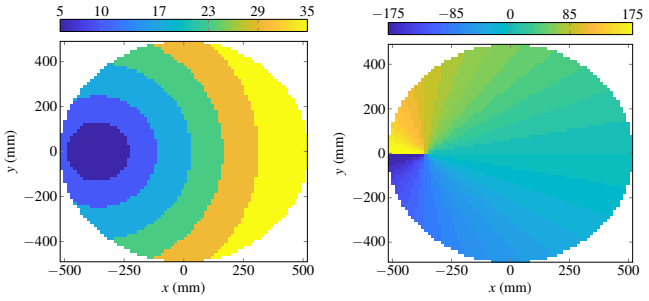

FIGURE 7. Discretization of the angles of incidence. (a) θ. (b) φ.

A. ANTENNA SPECIFICATIONS

A sketch of the antenna geometry is shown in Fig. 2. The considered reflectarray is elliptical, has a total of 4 068 elements in a regular grid with 74 and 70 cells in its main axes. The periodicity of the unit cell is 14 mm × 14 mm and the working frequency is 11.85 GHz. The feed is modeled as a $\cos^q\theta$ function with $q = 23$, generating an illumination taper of -17.9 dB. Also, the feed is placed at $\vec{r}_f = (-358, 0, 1070)$ mm, while the whole antenna is on a satellite in geostationary orbit at 10° E longitude. In addition, one SVM is trained per angle of incidence, which are discretized as shown in Fig. 7. This discretization guarantees a high accuracy in the computation of the radiation pattern with the SVM [29]. A total of 136 pairs of (θ, φ) angles are obtained, which are further reduced to 68 pairs using symmetries. For the unit cell, the bottom layer has a height of $h_A = 2.363$ mm and a complex relative permittivity $\varepsilon_{r,A} = 2.55 - j2.295 \cdot 10^{-3}$, while the top layer has a height of $h_B = 1.524$ mm and a complex relative permittivity $\varepsilon_{r,B} = 2.17 - j1.953 \cdot 10^{-3}$.

Fig. 8 shows the contour requirements for Europe with two coverage zones. This coverage is specified in the antenna coordinate system, and for the synthesis it must be transformed to the reflectarray coordinate system shown in Fig. 2 [2]. The copolar requirements are 28.5 dBi for zone 1 and 25.5 dBi for zone 2. The outer contours for each coverage zone represent the specifications taking into account typical satellite pointing errors: 0.1° in roll, 0.1° in pitch and 0.5° in yaw. The optimization will be carried out in dual-linear polarization using the same template specifications for both polarizations.

B. PHASE-ONLY SYNTHESIS

In the first step of the contoured beam reflectarray design, the generalized IA is used to obtain a phase distribution such that the desired copolar pattern is obtained for both linear polarizations. Since this is a local search algorithm, a suitable starting point is necessary to obtain good results. It has been demonstrated that a properly focused reflectarray provides a good starting point [39]. Thus, the initial phase distribution is given by [2]:

$$\angle\rho(x_k, y_k) = k_0 \left(d_k - (x_k \cos\varphi_0 + y_k \sin\varphi_0)\sin\theta_0\right), \qquad (21)$$

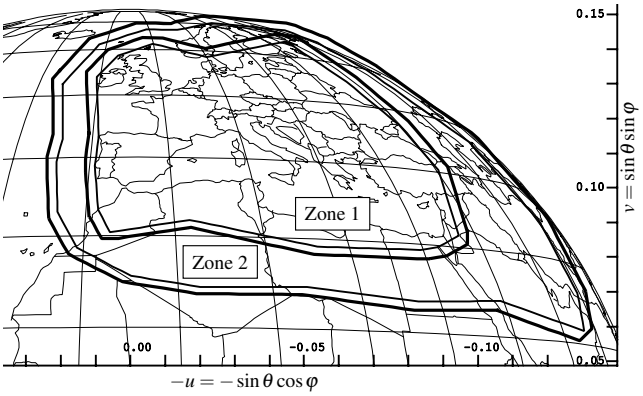

FIGURE 8. Europe footprint with two coverage zones for DBS application with (u,v) coordinates in the antenna coordinate system.

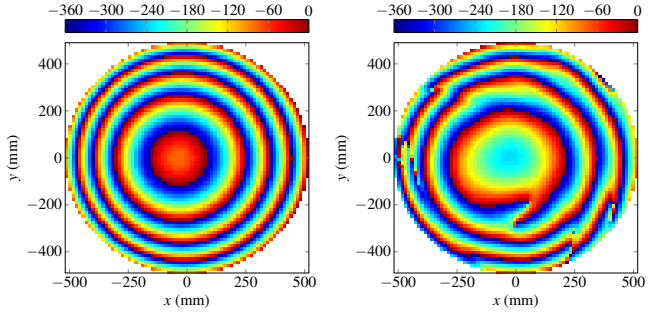

FIGURE 9. For polarization X: (a) starting phase distribution (deg) for the POS obtained with eq. (21) and (b) synthesized phase distribution (deg) after the POS with the generalized Intersection Approach.

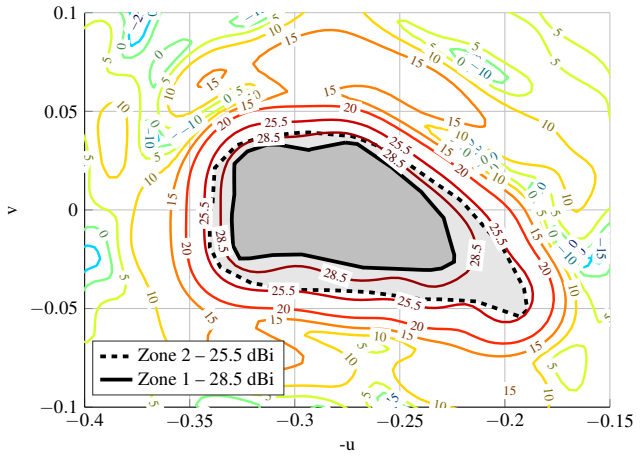

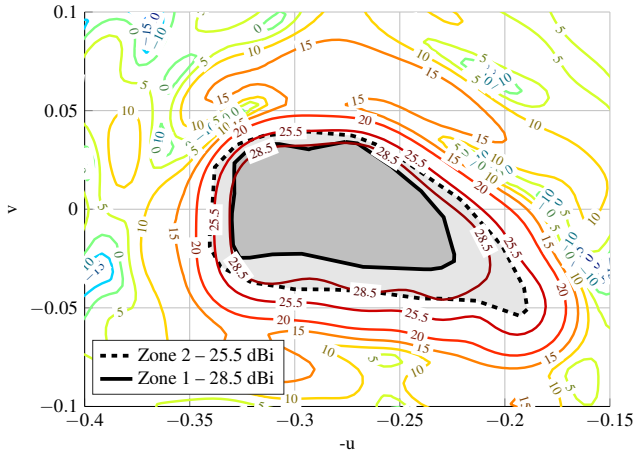

FIGURE 10. Copolar radiation pattern in dBi for (a) polarization X and (b) polarization Y when computed not taking into account the displacement of the unit cell phase shifters.

where $\angle\rho(x_k, y_k)$ corresponds to the phase of $\rho_{xx,k}$ in polarization X or $\rho_{yy,k}$ in polarization Y, (θ_0, φ_0) is the pointing direction of the reflectarray main beam, and d_k the distance between the kth reflectarray element and the phase center of the feed. Two phase distributions are needed, one for each linear polarization. In addition, the initial phase distribution will be different for both polarizations since the phase-shifters of the unit cell in Fig. 3 are shifted half period, so d_k in (21) will be different for both linear polarizations at the kth element.

The result from this step is two phase-distributions which generate the desired copolar pattern for both linear polarizations that comply with certain requirements. Fig. 9(a) shows the initial phase distribution for polarization X obtained with (21). It generates a pencil beam pointing at $(\theta_0, \varphi_0) = (16.6°, 0°)$, which approximately corresponds to the center of zone 1 in the reflectarray coordinate system. The phase distribution for Y polarization is similar. After the POS, the phase distribution of Fig. 9(b) is obtained for X polarization. It must be noted that these results were obtained taking into account the formulation for the spatial displacement of the dipoles for Y polarization. If this displacement is not taken into account, the radiation pattern would be shifted. However, this only occurs to polarization Y, and the copolar pattern of polarization X would remain the same [27], as shown in Fig. 10. The shift in the radiation pattern is close to 0.3°, and in the present case causes a significant drop in the minimum copolar gain, as it will be later evaluated. Another space application in which it is fundamental to consider this shift is in multibeam applications, where the spacing between adjacent beams is very narrow, of the order of 0.5°-0.6° [4].

C. LAYOUT DESIGN

Once the desired phase-shift has been obtained, the next step consists in finding the element dimensions that produce the required phase-shift for each linear polarization. The design procedure followed in this work is summarized in Fig. 11. For each reflectarray element, it performs the following steps. First, it generates a table of phase-shifts by varying T_x and T_y either with the MoM-LP tool or the SVM. This is done independently for each variable since the phase-shift is practically uncoupled for both variables [23]. We select two values for T_x and T_y which provide, for each case, a phase-shift which is above and below the objective value. Then, the estimated value of the length that provides the required

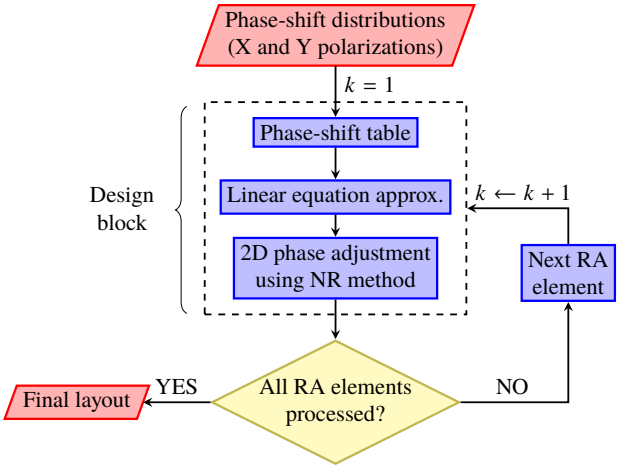

FIGURE 11. Flowchart of the design procedure from the required phase-shift to the final reflectarray layout.

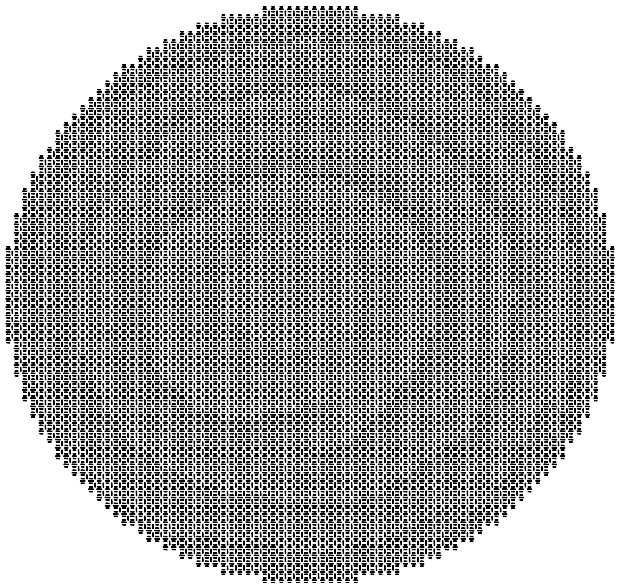

FIGURE 12. Initial layout for upper layer obtained from the phase distribution shown in Fig. 9(b).

phase-shift is obtained using a linear equation approximation. Finally, using a zero-finding routine, for instance the Newton-Raphson (NR) method, the exact value of T_x and T_y is sought, taking into account the coupling between phase-shifters that there may exist.

Following the aforementioned procedure and employing the unit cell shown in Fig. 3, the layout of Fig. 12 for the upper layer is obtained. When the layout is simulated with SVM, the radiation patterns shown in Fig. 13 are obtained for polarization X. As it can be seen, it perfectly complies with the specifications for the two coverages. Minimum copolar gain for zone 1 is 29.29 dBi while for zone 2 is 26.03 dBi. Similar results were obtained for polarization Y, where the minimum gain for zone 1 and 2 is 29.32 dBi and 26.03 dBi, respectively. These results were obtained taking into account the physical displacement of the phase-shifter for Y polarization. Otherwise, the copolar radiation pattern of Fig. 10 would be obtained, where the minimum copolar gain for Y polarization drops to 27.72 dBi and 24.00 dBi for zones 1 and 2, respectively, and thus not complying with the requirements after the POS.

The design has been carried out in a desktop computer with an Intel Core i7-7700 at 3.60 GHz with eight CPUs (four physical plus four virtual using hyperthreading). The procedure has been parallelized to use all available threads. With the MoM-LP it took 1 635.6 seconds (27 minutes and 15.6 seconds), while with SVM it took only 0.5 seconds, which supposes an acceleration factor of 3 271. When analysing the reflectarray layout comprised of 4 068 elements to obtain the $\mathbf{R}_k$ matrices, using MoM-LP took 57.6 seconds, while with SVM it took a mean time of 17.56 milliseconds, which supposes an acceleration factor of 3 279. Thus, both the analysis and design are accelerated more than three orders of magnitude using the SVM instead of the MoM-LP tool in the present case.

V. CROSSPOLAR OPTIMIZATION OF REFLECTARRAY ANTENNAS

A. CROSS-POLARIZATION PERFORMANCE

The cross-polarization performance of antennas for space applications such as DBS is usually measured with the crosspolar discrimination (XPD) and the crosspolar isolation (XPI). The XPD is defined, in linear scale, as the ratio point by point of the copolar and crosspolar gains for a certain coverage zone. Sometimes, the worst XPD value is considered, which corresponds to its minimum (XPD_{min}). On the other hand, the XPI is defined in linear scale as the ratio between the minimum copolar gain and the maximum crosspolar gain for a given coverage zone. Please note that due to their definition, the XPI is a stringent parameter than the XPD to evalute the cross-polarization performance in a coverage zone.

For the reflectarray designed in Section IV, the simulated layout with SVM gives a XPD_{min} of 31.46 dB for polarizations X and Y in zone 1, while they are 27.98 dB and 28.45 dB in zone 2 for polarizations X and Y, respectively. The lower value in zone 2 is mainly due to the lower value of the gain due to the copolar requirements. Similarly, the values for the XPI are 30.13 dB for polarizations X and Y in zone 1, and 25.92 dB and 26.44 dB in zone 2 for polarizations X and Y, respectively. Although the specifications for the XPD and XPI vary with the application, mission and even with the coverage zone [26], they typically demand values higher than 30 dB, which is not achieved in zone 2, and by a small margin in zone 1. Thus, the goal will be to improve the cross-polarization performance by carrying out an optimization of the reflectarray layout.

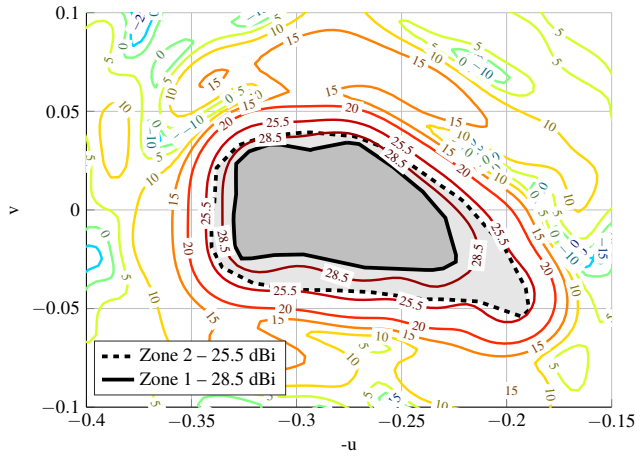

(a)

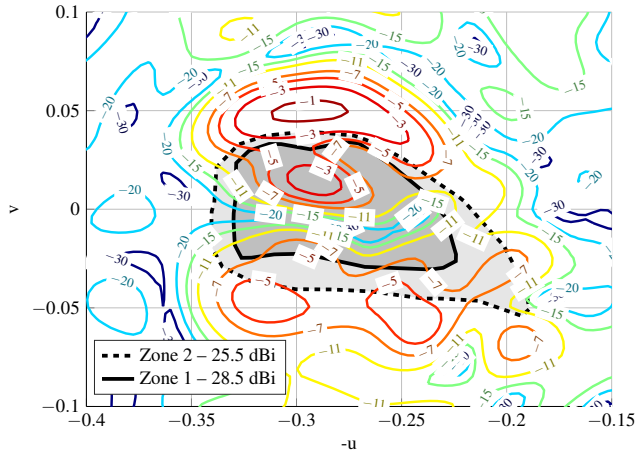

(b)

FIGURE 13. Radiation pattern in dBi for polarization X. (a) Copolar. (b) Crosspolar.

B. DIRECT OPTIMIZATION OF CROSS-POLARIZATION PARAMETERS

A direct optimization of the reflectarray layout to improve the cross-polarization performance presents some challenges with regard to the POS. First, the number of potential optimizing variables considerably grows, since the number of available degrees of freedom increases. This presents some drawbacks: although it has the potential to provide better results, the number of local minima grows exponentially with the number of variables, making convergence more difficult; and computationally, the algorithm becomes slower. In addition, in the POS for two linear polarizations, they can be synthesized independently, so the number of optimizing variables is just one per reflectarray element (the phase of ρ_{xx} or ρ_{yy}, depending on the polarization). This is not the case when optimizing the cross-polarization performance, since the radiation patterns for both linear polarizations depend on the whole $\mathbf{R}_k$ matrix, and thus at least two variables per element are required, while considering more components of the far field. To overcome those issues, a number of techniques were introduced in Sections II and III. The generalized Intersection Approach, with improved convergence properties, is able to handle tens of thousands of optimizing variables while achieving good results [21]. Also, SVMs were introduced to accelerate the reflectarray analysis and the DFC technique to speed up the computation of the gradient, which is typically the most time consuming operation in gradient-based local optimizers.

On the other hand, the usual approach to perform crosspolar optimization is to impose some requirements directly on the crosspolar pattern with the aim of reducing it [20], [21]. However, in some space applications, such as DBS, the figure of merit for cross-polarization performance is the XPD or the XPI. If the crosspolar pattern is optimized, the XPD and XPI are improved indirectly, providing suboptimal results. Thus, it is proposed to directly optimize the XPD and XPI in order to further improve the cross-polarization performance of the antenna [40].

The next step is to perform the crosspolar optimization using as starting point the layout designed in Section IV and shown in Fig. 12. For this task, two approaches will be employed: optimize the crosspolar pattern on the one hand, and the crosspolar discrimination or crosspolar isolation on the other hand. The aim is to show that, when the figure of merit for the cross-polarization performance of a reflectarray antenna is the XPD or XPI, it is best to directly optimize the figure of merit. For the crosspolar optimization, the same approach presented in [21] is employed, setting the crosspolar template in the forward projector (see Fig. 6) 40 dB below the maximum copolar gain. On the other hand, to improve the minimum value of the XPD_{min} in both coverage zones, a minimum template of 40 dB is set in substitution of the crosspolar template following [40]. The same applies to the optimization of the XPI.

The different approaches were tested with the generalized Intersection Approach, which was left to run 80 iterations until the error stagnated for a better comparison. The evolution of the XPD_{min} and XPI on the two coverage zones (see Fig. 8) for the three optimizations is shown in Fig. 14. As it can be seen, the presented strategy provides better results in the final value of XPD_{min} and XPI, which are better when they are directly optimized. For instance, for zone 1 the XPD_{min} reaches a value of 35.10 dB when optimizing the crosspolar pattern, but it improves to 39.64 dB and 39.53 dB when optimizing the XPD_{min} and XPI, respectively, in polarization X. This supposes an increment of more than 4 dB with the new proposed strategy over the usual approach, and more than 8 dB over the starting point (31.46 dB). This improvement occurs for both polarizations and both coverage zones as shown in Table 1, where the final results for the three optimization approaches are provided, including the minimum copolar gain in both coverage zones.

Fig. 15 shows the final radiation pattern for polarization X when the XPD_{min} is optimized. Comparing it with the radiation pattern at the starting point of Fig. 13, the copolar pattern is very similar, in fact it also complies with the requirements

TABLE 1. Results of the direct optimization using SVM of a reflectarray antenna with a European footprint with two coverage zones comparing different strategies: the usual approach of optimizing the crosspolar component of the radiation pattern (XP opt.) and the new strategy of directly optimizing the figure of merit (XPD_{min} opt. and XPI opt.). Values of CP_{min} are in dBi and values of XPD_{min} and XPI are in dB.

	Zone 1 (28.5 dBi)						Zone 2 (25.5 dBi)					
	Pol. X			Pol. Y			Pol. X			Pol. Y		
	CP_{min}	XPD_{min}	XPI	CP_{min}	XPD_{min}	XPI	CP_{min}	XPD_{min}	XPI	CP_{min}	XPD_{min}	XPI
Initial	29.29	31.46	30.13	29.32	31.46	30.13	26.03	27.98	25.92	26.03	28.45	26.44
XP opt.	29.30	35.10	34.57	29.26	35.60	33.38	26.27	31.85	31.11	26.31	31.63	31.07
XPD_{min} opt.	29.00	39.64	37.46	29.08	39.36	37.46	25.96	35.96	33.46	25.67	36.76	33.81
XPI opt.	29.04	39.53	39.25	29.01	40.32	39.00	25.80	34.78	34.49	26.06	36.29	35.75

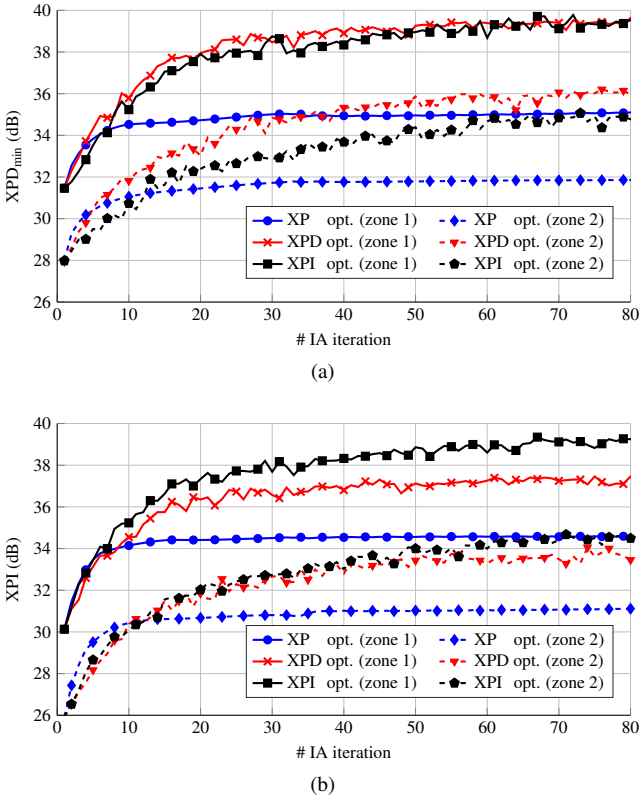

FIGURE 14. Evolution of the (a) XPD_{min} and (b) XPI for the three different optimization strategies studied in this work.

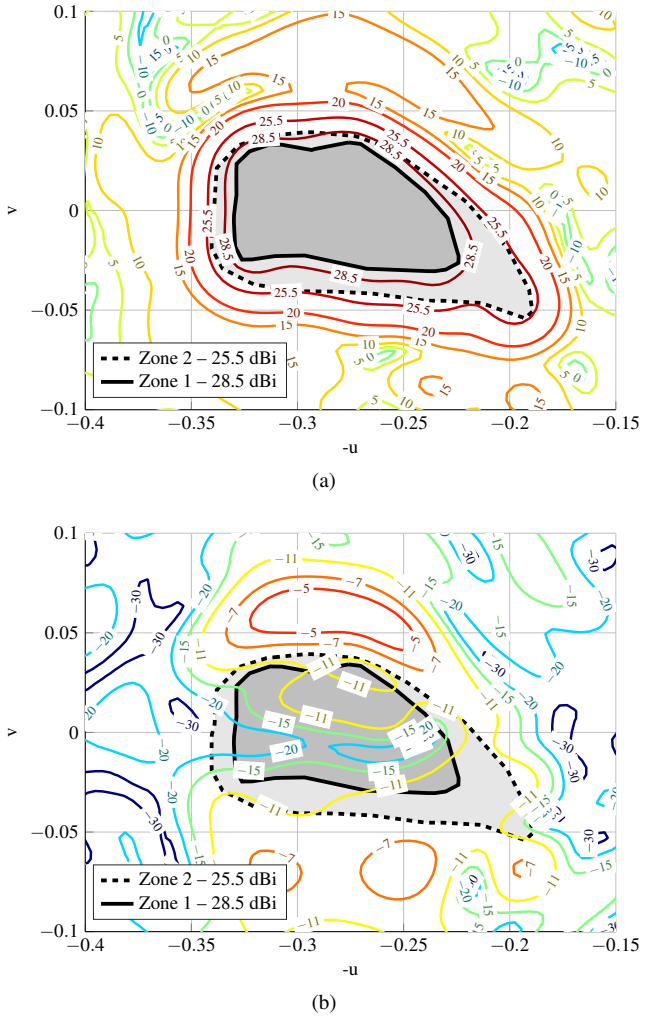

FIGURE 15. Obtained radiation pattern in dBi for polarization X after the XPD_{min} optimization. (a) Copolar. (b) Crosspolar.

after the optimization as shown in Table 1. The crosspolar pattern is now lower, specially inside the coverage zones where the XPD_{min} was considerably improved.

All the results shown in Table 1 were obtained using the SVM as simulation tool. To compare the SVM simulations with MoM-LP, the layout obtained after the XPI optimization using the SVM was also simulated with MoM-LP and the results are shown in Table 2. Two different MoM-LP simulations were carried out to study the source of discrepancies between the SVM and MoM-LP, one using the real angle of incidence at each reflectarray element, and another using the same discretization of the angles of incidence as the SVM (see Fig. 7). As it can be seen, when the layout is simulated using the same angles of incidence as the SVM, the differences between the SVM and MoM-LP predictions are reduced. In this case, the only source of discrepancy is the accuracy of the SVM model, which is demonstrated to be reliable [29]. Nevertheless, even when simulating with the real angles of incidence, the results are quite close to those

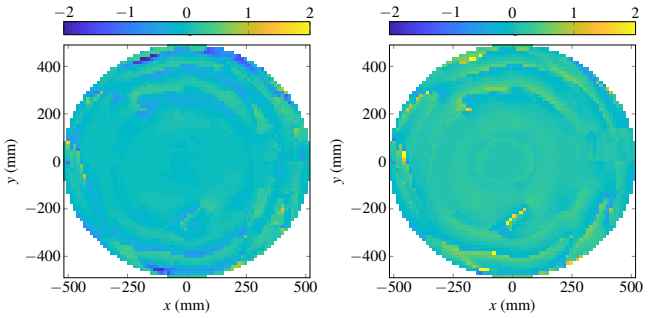

FIGURE 16. Differences in mm between the initial and optimized layout of the upper layer for (a) T_x and (b) T_y.

predicted by the SVM simulation. Since the optimization was carried out with the SVM, it is feasible to accelerate computations with the SVM and finally obtain a more accurate prediction with a single MoM-LP analysis.

All the optimizations were carried out at a single frequency. However, since reflectarrays have inherently a low bandwidth, it could be improved by performing optimization at several frequencies [14], [20] using the techniques presented in this work to considerably accelerate computations and improve the performance of the antenna.

Finally, Fig. 16 shows the differences in mm between the initial and optimized layout (upper layer, see Fig. 12) for the T_x and T_y variables as defined in Fig. 3. The maximum variation in T_x is 1.94 mm while in T_y is 2.74 mm. On the other hand, the mean absolute deviation for T_x is 0.15 mm while for T_y is 0.17 mm. Similar results were obtained for the bottom layer.

C. COMPUTATIONAL PERFORMANCE

This section provides a thorough account of the computational performance of the optimization framework introduced in this work, which employs the generalized IA algorithm and integrates a number of techniques that improve both, computational performance of the algorithm and cross-polarization performance of the antenna with regard to the baseline scenario [21]. On the one hand, the computational performance is greatly improved by using SVMs instead of MoM-LP for the reflectarray analysis during the optimization loop. In this regard, there is an initial one-time cost accounting for the 680 SVM trainings (68 angles and 10 coefficients per angle), that for the case at hand took less than an hour using a workstation; this is the case since the training of one SVM is independent from the rest and can be easily parallelized. A new training should be performed if the reflectarray element is changed, but the obtained SVMs may be used for multiple designs and optimizations with different radiation pattern requirements. In addition, the gradient computation is accelerated by using the technique of differential contributions (DFC). On the other hand, the final cross-polarization performance of the antenna is improved by directly optimizing the figure of merit, which it can be the XPD or XPI, depending on the application. Moreover, the memory footprint is also reduced with regard to the usual approach of directly optimizing the crosspolar pattern, and also the algorithm is slightly accelerated since the Jacobian matrix multiplication (see Fig. 6) is faster. All the results for the computational study of the optimization algorithm were obtained in a workstation with two Intel Xeon E5-2650v3, each with ten cores that handle a total of 40 threads at 2.3 GHz.

Table 3 shows the computational results for the building blocks of the LMA comparing several techniques. The FFT resolution is 512×512 and the number of points considered in the UV grid for the pattern optimization is $T = 11\,187$. Since two copolar and two crosspolar patterns are required for dual-linear polarized reflectarrays, the total number of points is $4T = 44\,748$. In addition, for the computation of the radiation patterns with the first principle of equivalence, eight spectrum functions are required, and two FFTs per spectrum functions are used using the analysis detailed in Section II, thus using a total of 16 FFTs in the computation of the far field.

In principle, the most time consuming operation to calculate the cost function is the analysis with MoM-LP to obtain $\mathbf{R}_k$. The DFC technique does not have any impact, since it only applies to the computation of the gradient (Jacobian matrix). Thus, the cost function is only accelerated with the SVM, which considerably speeds up the unit cell analysis. In fact, when only considering the computation of $\mathbf{R}_k$, the analysis is accelerated more than three orders of magnitude with regard to the MoM-LP simulation, as shown in Section IV. In the case of the cost function, also the computation of 16 FFTs needs to be included, which accounts for the remaining time shown in Table 3 and that are not accelerated by the SVM.

The Jacobian matrix computation is substantially accelerated by the combination of the SVM and DFC. By itself, the DFC technique accelerates the computation of the Jacobian, going from taking almost 91 seconds to approximately 62 seconds. Using only the SVM the computing time is almost reduced by half. However, combining both techniques, the gradient computation is accelerated more than one order of magnitude, reaching a speed up factor of 22.3 in the present case.

The matrix multiplication ($J^T J$) and the linear equation solver are not accelerated neither by the use of SVM nor DFC, so their computing time remain approximately the same. The matrix multiplication depends on the size of the Jacobian (total number of points in the UV grid times the number of optimizing variables) while the time of the solver only depends on the number of optimizing variables. The linear equation solver is based on the Cholesky decomposition, which is the fastest exact solver [31]. On the other hand, the matrix multiplication is now the slowest operation in the optimization process after the acceleration in the Jacobian matrix computation. However, the computing time shown in Table 3 corresponds to the classical approach of optimizing

TABLE 2. Comparison between the SVM and MoM-LP simulations of the layout obtained after the XPI optimization. For the MoM-LP simulation two cases are considered: using the real angles of incidence (MoM-LP), and the same angles of incidence as the SVM (MoM-LP; SVM angles). Values of CP_{min} are in dBi and values of XPD_{min} and XPI are in dB.

	Zone 1 (28.5 dBi)						Zone 2 (25.5 dBi)					
	Pol. X			Pol. Y			Pol. X			Pol. Y		
	CP_{min}	XPD_{min}	XPI	CP_{min}	XPD_{min}	XPI	CP_{min}	XPD_{min}	XPI	CP_{min}	XPD_{min}	XPI
SVM	29.04	39.53	39.25	29.01	40.32	39.00	25.80	34.78	34.49	26.06	36.29	35.75
MoM-LP	28.78	39.56	38.47	29.02	39.01	38.30	25.85	34.15	33.04	26.05	34.85	34.33
MoM-LP (SVM angles)	29.04	39.55	39.46	29.02	40.91	39.24	25.81	35.17	34.56	26.05	35.71	35.54

TABLE 3. Computational time study of the optimization algorithm for an FFT resolution of 512×512 (44 748 points considered in the optimization) and 7 993 optimizing variables. All values are in seconds.

Tool	Cost function	Jacobian	J^TJ	Solver
MoM-LP	30.08	90.73	17.66	1.20
MoM-LP + DFC	30.08	61.77	19.23	1.22
SVM	0.22	48.30	17.73	1.21
SVM + DFC	0.22	4.06	18.77	1.22

TABLE 4. Computational time study of the optimization algorithm for an FFT resolution of 128×128 (2 800 points considered in the optimization) and 7 993 optimizing variables. All values are in seconds.

Tool	Cost function	Jacobian	J^TJ	Solver
MoM-LP	30.05	61.20	1.22	1.20
MoM-LP + DFC	29.99	59.22	1.17	1.20
SVM	0.13	3.77	1.42	1.18
SVM + DFC	0.13	0.65	1.38	1.20

the crosspolar pattern. When the XPD or XPI are optimized, the number of points in the UV are reduced, since only one cross-polarization parameter is taken into account per coverage zone. If T is the number of points in which the copolar pattern is computed and P is the total number of optimizing variables, the size of the Jacobian is reduced from $4T \times P$ when optimizing the crosspolar pattern to $\sim 2T \times P$ when optimizing the XPD_{min} or XPI. So not only the memory footprint is approximately reduced by half, the matrix multiplication computing time is also reduced. For the present case, this time is reduced to 9.51 seconds. Thus, the time per iteration goes from approximately 140 seconds of the standard approach to 15 seconds, a total acceleration of one order of magnitude per iteration for the optimization process when all techniques presented in this work are employed at the same time.

Finally, Table 4 shows the same computing time study for a reduced FFT resolution, which is now 128×128. Although such low number of UV points does not provide enough resolution for highly directive reflectarrays, it may be enough for some small or medium sized antennas. Since now the FFT is considerably faster than in the previous case, the acceleration provided by the DFC technique has less impact in the overall acceleration, where the SVM plays a more important role. In addition, the Jacobian size is considerably reduced, and thus the matrix multiplication is faster. Since the number of optimizing variables is the same, the linear equation solver takes the same time. The time per iteration is now reduced from 97 seconds to 3.4 seconds, an acceleration factor close to 30.

VI. CONCLUSIONS

This paper has presented a general and efficient framework for the optimization of very large reflectarrays for space applications. It is based on a two-step procedure, both using the generalized Intersectation Approach. The first step consists of a Phase-Only Synthesis (POS) which provides a good starting point for the second step, where the crosspolar optimization is carried out. With the aim of accelerating computations and improving antenna performance, three strategies are employed. First, a machine learning algorithm based on Support Vector Machines (SVMs), is used to obtain a surrogate model of the reflectarray unit cell. This model is used in substitution of a full-wave analysis tool based on local periodicity, accelerating reflectarray analysis by more than three orders of magnitude without compromising accuracy. Then, the technique of differential contributions on the radiated field is employed to substantially accelerate the computation of the gradient in array optimization. This novel technique is based on the linearity of Maxwell's equations, which provides a linear relation between the tangential field at the aperture and the radiated field (either near or far field). In this way, only the contribution of one element is taken into account for the computation of each column of the Jacobian matrix, saving time. Finally, antenna performance is improved by directly optimizing the figure of merit of interest, either the crosspolar discrimination (XPD) or crosspolar isolation (XPI), instead of the crosspolar pattern, which is the usual approach.

This framework has been tested on a very large reflectarray for a DBS mission with a European footprint and two coverage zones, working in dual-linear polarization. The first step provides a layout that fully complies with the copolar gain

requirements in both coverage zones and polarizations. Then, a direct optimization of the reflectarray layout is performed to improve the cross-polarization performance. Three approaches are compared: optimation of the crosspolar pattern, XPD_{min} and XPI. It is shown that directly optimizing the figure of merit (XPD_{min} or XPI) provides better results in less time than the usual strategy of optimizing the crosspolar pattern. With regard to the starting point, the XPD_{min} and XPI are improved more than 9 dB and 7 dB, respectively, while maintaining the copolar pattern within specifications. Finally, a study of the computational improvements of the techniques described in this work is presented. The reflectarray analysis and design are accelerated more than three orders of magnitude thanks to the use of SVMs while keeping a high degree of agreement with MoM-LP simulations. On the other hand, when SVMs and DFC are combined, the time per iteration of the crosspolar optimization is accelerated more than one order of magnitude.

ACKNOWLEDGMENT

The authors would like to thank Prof. J. A. Encinar and Prof. R. R. Boix for the fruitful technical discussions on reflectarray analysis.

REFERENCES

[1] W. A. Imbriale, S. Gao, and L. Boccia, Eds., Space Antenna Handbook. Hoboken, NJ, USA: John Wiley & Sons, 2012.

[2] J. Huang and J. A. Encinar, Reflectarray Antennas. Hoboken, NJ, USA: John Wiley & Sons, 2008.

[3] D. R. Prado, A. Campa, M. Arrebola, M. R. Pino, J. A. Encinar, and F. Las-Heras, "Design, manufacture and measurement of a low-cost reflectarray for global Earth coverage," IEEE Antennas Wireless Propag. Lett., vol. 15, pp. 1418–1421, 2016.

[4] E. Martínez-de-Rioja, J. A. Encinar, A. Pino, B. González-Valdés, S. V. Hum, and C. Tienda, "Bifocal design procedure for dual reflectarray antennas in offset configurations," IEEE Antennas Wireless Propag. Lett., vol. 17, no. 8, pp. 1421–1425, Aug. 2018.

[5] C. Tienda, M. Younis, P. López-Dekker, and P. Laskowski, "Ka-band reflectarray antenna system for SAR applications," in The 8th European Conference on Antennas and Propagation (EUCAP), The Hague, The Netherlands, Apr. 6–11, 2014, pp. 1603–1606.

[6] D. R. Prado, M. Arrebola, M. R. Pino, and F. Las-Heras, "Improved reflectarray phase-only synthesis using the generalized intersection approach with dielectric frame and first principle of equivalence," Int. J. Antennas Propag., vol. 2017, pp. 1–11, May 2017.

[7] J. A. Zornoza and J. A. Encinar, "Efficient phase-only synthesis of contoured-beam patterns for very large reflectarrays," Int. J. RF Microw. Comput. Eng., vol. 14, no. 5, pp. 415–423, Sep. 2004.

[8] A. Capozzoli, C. Curcio, A. Liseno, and G. Toso, "Fast, phase-only synthesis of aperiodic reflectarrays using NUFFTs and CUDA," Progr. Electromagn. Res., vol. 156, pp. 83–103, 2016.

[9] D.-C. Chang and M.-C. Huang, "Multiple-polarization microstrip reflectarray antenna with high efficiency and low cross-polarization," IEEE Trans. Antennas Propag., vol. 43, no. 8, pp. 829–834, Aug. 1995.

[10] H. Hasani, M. Kamyab, and M. Ali, "Low cross-polarization reflectarray antenna," IEEE Trans. Antennas Propag., vol. 59, no. 5, pp. 1752–1756, May 2011.

[11] J. A. Encinar and M. Arrebola, "Reduction of cross-polarization in contoured beam reflectarrays using a three-layer configuration," in IEEE Antennas and Propagation Society International Symposium, Honolulu, Hawaii, USA, Jun. 9–15, 2007, pp. 5303–5306.

[12] C. Tienda, J. A. Encinar, M. Arrebola, M. Barba, and E. Carrasco, "Design, manufacturing and test of a dual-reflectarray antenna with improved bandwidth and reduced cross-polarization," IEEE Trans. Antennas Propag., vol. 61, no. 3, pp. 1180–1190, Mar. 2013.

[13] R. Florencio, J. A. Encinar, R. R. Boix, G. Pérez-Palomino, and G. Toso, "Cross-polar reduction in reflectarray antennas by means of element rotation," in 10th European Conference on Antennas and Propagation (EuCAP), Davos, Switzerland, Apr. 10–15, 2016, pp. 1–5.

[14] J. A. Encinar, M. Arrebola, L. F. de la Fuente, and G. Toso, "A transmit-receive reflectarray antenna for direct broadcast satellite applications," IEEE Trans. Antennas Propag., vol. 59, no. 9, pp. 3255–3264, Sep. 2011.

[15] O. M. Bucci, A. Capozzoli, G. D'Elia, and S. Musto, "A new approach to the power pattern synthesis of reflectarrays," in Proc. URSI International Symposium on Electromagnetic Theory (EMTS'04), Pisa, Italy, May 23–27, 2004, pp. 1053–1055.

[16] O. M. Bucci, A. Capozzoli, G. D'Elia, and S. Russo, "Power pattern synthesis of reflectarrays: comparison between two approaches," in Proc. of the XV Riunione Nazionale di Elettromagnetismo (CD-ROM), Cagliari, Italy, Sep. 13–16, 2004, pp. 1–4.

[17] ——, "An advanced technique for reflectarray power pattern synthesis and its experimental validation," in Proc. of the International Symposium on Antennas and Propagation (ISAP), Seoul, South Korea, Aug. 3–5, 2005, pp. 561–564.

[18] D. R. Prado, M. Arrebola, M. R. Pino, and F. Las-Heras, "Complex reflection coefficient synthesis applied to dual-polarized reflectarrays with cross-polar requirements," IEEE Trans. Antennas Propag., vol. 63, no. 9, pp. 3897–3907, Sep. 2015.

[19] H. Legay, D. Bresciani, E. Labiole, R. Chiniard, and R. Gillard, "A multi facets composite panel reflectarray antenna for a space contoured beam antenna in Ku band," Progr. Electromagn. Res. B, vol. 54, pp. 1–26, Aug. 2013.

[20] M. Zhou, S. B. Sørensen, O. S. Kim, E. Jørgensen, P. Meincke, and O. Breinbjerg, "Direct optimization of printed reflectarrays for contoured beam satellite antenna applications," IEEE Trans. Antennas Propag., vol. 61, no. 4, pp. 1995–2004, Apr. 2013.

[21] D. R. Prado, M. Arrebola, M. R. Pino, R. Florencio, R. R. Boix, J. A. Encinar, and F. Las-Heras, "Efficient crosspolar optimization of shaped-beam dual-polarized reflectarrays using full-wave analysis for the antenna element characterization," IEEE Trans. Antennas Propag., vol. 65, no. 2, pp. 623–635, Feb. 2017.

[22] W. L. Stutzman and G. A. Thiele, Antenna Theory and Design, 3rd ed. Hoboken, NJ, USA: John Wiley & Sons, 2012.

[23] R. Florencio, J. A. Encinar, R. R. Boix, V. Losada, and G. Toso, "Reflectarray antennas for dual polarization and broadband telecom satellite applications," IEEE Trans. Antennas Propag., vol. 63, no. 4, pp. 1234–1246, Apr. 2015.

[24] R. Florencio, R. R. Boix, and J. A. Encinar, "Enhanced MoM analysis of the scattering by periodic strip gratings in multilayered substrates," IEEE Trans. Antennas Propag., vol. 61, no. 10, pp. 5088–5099, Oct. 2013.

[25] E. M. de Rioja, J. A. Encinar, M. Barba, R. Florencio, R. R. Boix, and V. Losada, "Dual polarized reflectarray transmit antenna for operation in Ku- and Ka-bands with independent feeds," IEEE Trans. Antennas Propag., vol. 65, no. 6, pp. 3241–3246, Jun. 2017.

[26] J. A. Encinar, R. Florencio, M. Arrebola, M. A. Salas-Natera, M. Barba, J. E. Page, R. R. Boix, and G. Toso, "Dual-polarization reflectarray in Ku-band based on two layers of dipole arrays for a transmit-receive satellite antenna with South American coverage," Int. J. Microw. Wirel. Technol., vol. 10, no. 2, pp. 149–159, 2018.

[27] J. A. Encinar, M. A. Salas-Natera, M. Barba, M. Arrebola, D. R. Prado, R. R. Boix, and R. Florencio, "Reflectarray antennas with improved performances and design techniques. Final report," European Space Agency, Tech. Rep., Jun. 2016.

[28] B. Schölkopf and A. J. Smola, Learning with Kernels, 1st ed. Cambridge, Massachusetts: The MIT Press, 2001.

[29] D. R. Prado, J. A. López-Fernández, G. Barquero, M. Arrebola, and F. Las-Heras, "Fast and accurate modeling of dual-polarized reflectarray unit cells using support vector machines," IEEE Trans. Antennas Propag., vol. 66, no. 3, pp. 1258–1270, Mar. 2018.

[30] O. M. Bucci, G. D'Elia, G. Mazzarella, and G. Panariello, "Antenna pattern synthesis: a new general approach," Proc. IEEE, vol. 82, no. 3, pp. 358–371, Mar. 1994.

[31] D. R. Prado, J. Álvarez, M. Arrebola, M. R. Pino, R. G. Ayestarán, and F. Las-Heras, "Efficient, accurate and scalable reflectarray phase-only synthesis based on the Levenberg-Marquardt algorithm," Appl. Comp. Electro. Society Journal, vol. 30, no. 12, pp. 1246–1255, Dec. 2015.

[32] D. R. Prado, M. Arrebola, M. R. Pino, and F. Las-Heras, "Improving convergence in crosspolar optimization of reflectarray antennas," in 11th

European Conference on Antennas and Propagation (EuCAP), Paris, France, Mar. 19–24, 2017, pp. 100–103.
[33] J. Álvarez, R. G. Ayestarán, G. León, L. F. Herrán, A. Arboleya, J. A. López-Fernández, and F. Las-Heras, "Near field multifocusing on antenna arrays via non-convex optimisation," IET Microw. Antennas Propag., vol. 8, no. 10, pp. 754–764, Jul. 2014.
[34] T. H. Ismail, D. I. Abu-Al-Nadi, and M. J. Mismar, "Phase-only control for antenna pattern synthesis of linear arrays using the Levenberg-Marquardt algorithm," Electromagnetics, vol. 24, no. 7, pp. 555–564, 2004.
[35] M. Bakr, A. Elsherbeni, and V. Demir, Adjoint sensitivity analysis of high frequency structures with MATLAB®. Edison, NJ, USA: SciTech Publishing, 2017.
[36] M. Ghassemi, M. Bakr, and N. Sangary, "Antenna design exploiting adjoint sensitivity-based geometry evolution," IET Microw. Antennas Propag., vol. 7, no. 4, pp. 268–276, Mar. 2013.
[37] S. Koziel and A. Bekasiewicz, "Fast EM-driven size reduction of antenna structures by means of adjoint sensitivities and trust regions," IEEE Antennas Wireless Propag. Lett., vol. 14, pp. 1681–1684, 2015.
[38] D. R. Prado, A. F. Vaquero, M. Arrebola, M. R. Pino, and F. Las-Heras, "Acceleration of gradient-based algorithms for array antenna synthesis with far field or near field constraints," IEEE Trans. Antennas Propag., vol. 66, no. 10, pp. 5239–5248, Oct. 2018.
[39] J. A. Encinar and J. A. Zornoza, "Three-layer printed reflectarrays for contoured beam space applications," IEEE Trans. Antennas Propag., vol. 52, no. 5, pp. 1138–1148, May 2004.
[40] D. R. Prado and M. Arrebola, "Effective XPD and XPI optimization in reflectarrays for satellite missions," IEEE Antennas Wireless Propag. Lett., vol. 17, no. 10, pp. 1856–1860, Oct. 2018.

Daniel R. Prado was born in Sama de Langreo, Asturias, Spain, in 1986. He received the B.Sc., M.Sc., and Ph.D. degrees in telecommunication engineering from the University of Oviedo, Gijón, Spain, in 2011, 2012, and 2016, respectively.

From 2010 to 2011, he was with The Institute of Electronics, Communications and Information Technology, Queen's University Belfast, Belfast, U.K., where he was involved in the design of leaky-wave antennas as part of his B.Sc. research project. From 2011 to 2017, he was a Research Assistant with the Signal Theory and Communications Area, University of Oviedo, where he was involved in the development of efficient techniques for the analysis and synthesis of reflectarray antennas. In 2014, he was with the School of Electrical Engineering, KTH Royal Institute of Technology, Stockholm, Sweden, as a Visiting Scholar, where he was involved in transformation optics applied to dielectric lenses. Since 2018, he has been with the Institute of Sensors, Signals and Systems, Heriot-Watt University, Edinburgh, U.K. His current research interests include the analysis of nonuniform arrays and the development of efficient techniques for the analysis and optimization of near and far fields of reflectarray antennas.

Dr. Prado was a recipient of a Predoctoral Scholarship financed by the Gobierno del Principado de Asturias and a Postdoctoral Fellowship partially financed by the European Union.

Jesús A. López-Fernández was born in Avilés, Asturias, Spain. He received the M.Sc. and the Ph.D. degrees in telecommunication engineering from the University of Vigo, Spain, in 1999 and 2009, respectively.

From April 2002 to March 2003, he was a Marie-Curie Visiting Fellow at the Mechanical & Manufacturing Engineering Department, Trinity College Dublin (TCD). Since October 2003, he has been with the Electrical Engineering Department, University of Oviedo, Asturias, Spain, where he is currently an Associate Professor teaching courses on Digital Communications and Radar Systems. His research interests include iterative methods and speed-up schemes applied to scattering problems, parallel algorithms, and signal processing techniques.

Manuel Arrebola (S'99–M'07–SM'17) was born in Lucena (Córdoba), Spain. He received the M.Sc. degree in telecommunication engineering from the University of Málaga, Málaga, Spain, in 2002, and the Ph.D. degree from the Technical University of Madrid (UPM), Madrid, Spain, in 2008.

From 2003 to 2007, he was with the Electromagnetism and Circuit Theory Department, UPM, as a Research Assistant. In 2005, he was with the Microwave Techniques Department, Universität Ulm, Ulm, Germany, as a Visiting Scholar. In 2007, he joined the Electrical Engineering Department, Universidad de Oviedo, Gijón, Spain, where he is currently an Associate Professor. In 2009, he enjoyed a two-month stay at the European Space Research and Technology Centre, European Space Agency, Noordwijk, The Netherlands. In 2018, he was a Visiting Professor with the Edward S. Rogers Sr. Department of Electrical & Computer Engineering, University of Toronto, Toronto, Canada. His current research interests include the development of efficient analysis, design and optimization techniques of reflectarray and transmitarray antennas both in near and far field.

Dr. Arrebola was a co-recipient of the 2007 S. A. Schelkunoff Transactions Prize Paper Award given by the IEEE Antennas and Propagation Society.

Marcos R. Pino was born in Vigo, Spain, in 1972. He received the M.Sc. and Ph.D. degrees in telecommunication engineering from the University of Vigo, Vigo, Spain, in 1997 and 2000, respectively.

During 1998, he was a Visiting Scholar with the ElectroScience Laboratory, The Ohio-State University, Columbus, OH, USA. From 2000 to 2001, he was an Assistant Professor with the University of Vigo. Since 2001, he has been with the Electrical Engineering Department, University of Oviedo, Gijón, Spain, where he is currently an Associate Professor teaching courses on communication systems and antenna design. His current research interests include antenna design, measurement techniques, and efficient computational techniques applied to EM problems, such as evaluation of radar cross section or scattering from rough surfaces.

George Goussetis (S'99–M'02–SM'12) received the Diploma degree in electrical and computer engineering from the National Technical University of Athens, Athens, Greece, in 1998 and the Ph.D. degree from the University of Westminster, London, UK, in 2002. In 2002 he also graduated B.Sc. in physics (first class) from University College London (UCL), London, U.K.

In 1998, he joined Space Engineering, Rome, Italy, as an RF Engineer. In 1999, he joined the Wireless Communications Research Group, University of Westminster, as a Research Assistant. Between 2002 and 2006, he was a Senior Research Fellow at Loughborough University, Loughborough, U.K. He was a Lecturer (Assistant Professor) with Heriot-Watt University, Edinburgh, U.K., between 2006 and 2009, and a Reader (Associate Professor) with Queen's University Belfast, U.K., between 2009 and 2013. In 2013, he joined Heriot-Watt University as a Reader and was promoted to Professor in 2014, where he currently directs the Institute of Sensors, Sigals and Systems. He has authored or co-authored over 500 peer-reviewed papers, five book chapters, and one book. He holds four patents. His current research interests include microwave and antenna components and subsystems.

Dr. Goussetis was a recipient of a Research Fellowship from the Onassis Foundation in 2001, the U.K. Royal Academy of Engineering from 2006 to 2011, and the European Marie-Curie Experienced Researcher Fellowships from 2011 to 2012 and from 2014 to 2017. He was a co-recipient of the 2011 European Space Agency Young Engineer of the Year Prize, the 2011 EuCAP Best Student Paper Prize, the 2012 EuCAP Best Antenna Theory Paper Prize, and the 2016 Bell Labs Prize. He has served as an Associate Editor for the IEEE Antennas and Wireless Propagation Letters.